PCCP

Accepted Manuscript

ROYAL SOCIETY OF CHEMISTRY

www.rsc.org/pccp

Journal Name

ARTICLE

Carbon Nanodot Decorated Graphitic Carbon Nitride: New Insights on the Enhanced Photocatalytic Water Splitting from ab-initio Studies

Received 00th January 20xx,
Accepted 00th January 20xx

DOI: 10.1039/x0xx00000x

www.rsc.org/

Guoping Gao[a], Yan Jiao[b], Fengxian Ma[a], Yalong Jiao[a], Eric Waclawik[a], and Aijun Du[a,*]

Interfacing carbon nanodots (C-dots) with graphitic carbon nitride (g-C_3N_4) produces a metal-free system that has recently demonstrated significant enhancement of photo-catalytic performance for water splitting into hydrogen [*Science*, 2015, **347**, 970-974]. However, the underlying photo-catalytic mechanism is not fully established. Herein, we have carried out density functional theory (DFT) calculations to study the interactions between g-C_3N_4 and trigonal/hexagonal shaped C-dots. We find that hybrid C-dots/g-C_3N_4 can form a type-II van der Waals heterojunction, leading to significant reduction of band gap. The C-dot decorated g-C_3N_4 enhances the separation of photogenerated electron and hole pairs and the composite's visible light response. Interestingly, the band alignment of C-dots and g-C_3N_4 calculated by hybrid functional method indicates that C-dots act as a spectral sensitizer in hybrid C-dots/g-C_3N_4 for water splitting. Our results offer new theoretical insights on this metal-free photocatalyst for water splitting.

Introduction

Producing hydrogen by photocatalytic water splitting is considered as a promising method to solve current energy and environmental issues[1]. Fujishima *et al.* first realized photocatalytic water splitting by a single-crystal TiO_2 anode and a Pt cathode.[2] Following this work, various metal-based semi-conductor materials[3], including metal (oxy) sulphide, metal (oxy) nitride catalysts have been demonstrated that have the capability for photocatalytic water splitting. To obtain an ideal photocatalyst, the following criteria should be taken into account[4-6]: (i) a narrow band gap with excellent visible-light response; (ii) band alignment suitable for overall water splitting, i.e. the valence band maximum (VBM) should be more positive than the standard electrode potential of H_2O/O_2 (1.23 eV vs NHE) or H_2O_2/O_2 (1.78 eV vs NHE), while the conduction band minimum (CBM) should be more negative than the standard electrode potential H^+/H_2 (0 eV vs NHE); (iii) efficient charge separation and transfer rate; (iv) enough number of activity sites for H^+ reduction and H_2O oxidation; and (v) stability. However, no catalysts obtained so far can satisfy all these criteria.

Since the pioneering work by Wang *et al.* on the visible-light photocatalytic water splitting based graphitic carbon nitride in the presence of a sacrificial donor[7], g-C_3N_4 has attracted extensive attention from both experiments and theoretical calculations[8]. g-C_3N_4 is a low cost photocatalyst, and shows high stability in both acidic and alkaline conditions. However, the relative large band gap of pristine g-C_3N_4 limits its visible-light absorption[9]. Furthermore, the low charge mobility of this material leads to fast recombination of photo induced electron-hole pairs.[10, 11] In addition, the nature of covalent bonding in g-C_3N_4 leads to low H^+ reduction and H_2O oxidation efficiencies on its surface.[12] A number of strategies which could modify the valence band (VB)/conduction band (CB) positions of g-C_3N_4, are applied to improve the visible-light photocatalytic water splitting performance of g-C_3N_4, including heteroatom doping[13, 14], hybridizing g-C_3N_4 with other nanomaterials[15-18] or molecules [19]. On the other hand, the C-dots offer certain of advantages in water solution photocatalysis, low toxicity, and

[a] School of Chemistry, Physics and Mechanical Engineering, Queensland University of Technology (QUT), Garden Point Campus, QLD 4001, Brisbane, Australia,
[b] School of Chemical Engineering, University of Adelaide, Adelaide, SA 5005, Australia
* Corresponding Author: Aijun Du, aijun.du@qut.edu.au
Electronic Supplementary Information (ESI) available: Band structure for 1x1 g-C3N4 based on hybrid functional. See DOI: 10.1039/x0xx00000x

tuneable emissions from near-infrared to blue wavelengths has motivated many efforts to utilize the as photocatalysts.[20] For example, Kang *et al.* have reported on a series of C-dot based photocatalysts with excellent catalytic activity.[21, 22] Zhang *et al.* proved that the zigzag edges of C-dots is more important than the armchair edges for light adsorption in visible light range.[23]

More recently, Liu *et al.* have demonstrated that the fabrication of metal-free *g*-C_3N_4 combined with C-dots showed impressive performance for photocatalytic solar water splitting[16]. However, the possible mechanism underneath is still not clear. In this paper, we have explored the interaction of C-dots and *g*-C_3N_4, and their electronic and optical properties by first-principle calculations. Our results demonstrate that, hybrid C-dots/*g*-C_3N_4 can form a type-II van der Waals heterojunction with a significant reduction of the band gap, which favours the separation of photogenerated electron and hole pairs, and leads to a red shift in light absorption in the hybrid systems. The C-dots act as spectral sensitizer in hybrid C-dots/*g*-C_3N_4 for splitting water into hydrogen.

Computational method

DFT calculations were performed by using the Vienna *Ab-initio* Simulation Package (VASP).[24, 25] The exchange-correlation interactions were described by generalized gradient approximation (GGA)[26] with the Perdew-Burke-Ernzerhof (PBE) functional[27]. Spin-polarization was included in all the calculations and a damped van der Waals correction was incorporated using Grimme's scheme to better describe the non-bonding interactions[28] . The cut-off energies for plane waves were set to be 500 eV, and the residual force and energy on each atom during structure relaxation were converged to 0.005 eV/Å and 10^{-5} eV, respectively. The vacuum space was more than 20 Å, which was enough to avoid the interaction between periodical images. The lattice constant of *g*-C_3N_4 was calculated to be 6.95 Å. The Brillouin zone was sampled with the Monkhorst−Pack mesh[29] with a K-point of 6 × 6 × 1 grid in reciprocal space during geometry optimization and electronic structure calculations. The K-point was increased to 11 × 11 × 1 to obtain the accurate optical absorption spectra. The hybrid functional (HSE06)[30] was employed to obtain the more accurate vacuum potential levels of *g*-C_3N_4 and C-dots. The potential level vs NHE was converted from vacuum potential level by the following Eq (1)[31]:

$$E_{potential\ level\ vs\ NHE} = -4.44 - E_{vacuum\ potential\ level} \quad (1)$$

The interaction energy between C-dot and *g*-C_3N_4 was calculated by Eq (2):

$$E_{interaction} = E_{nanodot/g-C_3N_4} - E_{nanodot} - E_{g-C_3N_4} \quad (2)$$

, where $E_{nanodot/g-C_3N_4}$, $E_{nanodot}$, and $E_{g-C_3N_4}$ represent the total energy of hybrid system, isolated C-dot, and isolated *g*-C_3N_4, respectively.

Results and analysis

Two groups of C-dots in different shapes and size, namely trigonal C-dots (Figure 1 a-c) and hexagonal C-dots (Figure 1 d-e) with zigzag-edges are first constructed. All the edge-carbon atoms are terminated by one hydrogen atom. Geometry optimization was then performed by using the conjugated gradient method. Figure 1 a-e presents the fully optimized structures for C-dots and *g*-C_3N_4, respectively. The equilibrium geometry for *g*-C_3N_4 in a 2x2 unit cell is given in Figure 1f.

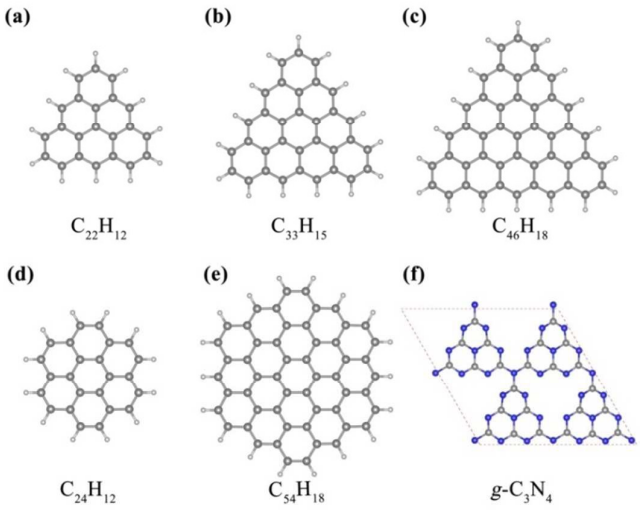

Figure 1 The optimized structures of trigonal C-dots (a-c), hexagonal C-dots (d-e), and *g*-C_3N_4 (f). Atom colour code: carbon (grey), nitrogen (blue), hydrogen (white). Molecule sizes are not drawn to scale.

In the following context, the effects of C-dots in the C-dots/*g*-C_3N_4 are investigated by calculating their band structures as shown in Figure 2. The trigonal C-dot and hexagonal C-dot used here are $C_{22}H_{12}$ and $C_{24}H_{12}$, respectively. Different adsorption sites for the C-dots on the surface of *g*-C_3N_4 in a 2x2 unit cell are calculated to construct the most energy-favour hybrid systems. The interlayer distance between *g*-C_3N_4 and C-dots are around 3.2 Å in both the stable hybrid systems. The closest atoms among periodical C-dots in both systems are edge hydrogens and the distances are above 4.5 Å, which is much larger twice of the Van der Waals Radii of hydrogen (1.2 Å)[32]. Therefore, the unit of 2x2 *g*-C_3N_4 is big enough to avoid the interaction of periodical C-dots.

An accurate band structure of 1 x 1 *g*-C_3N_4 was also obtained by the HSE06 method (see Figure S1 in the supplementary information). Here we should emphasize that standard density functional method is used for the band structure calculations because the hybrid systems are relatively large and the HSE06 calculation is very computational demanding. For the purpose of comparison, the contributions of C-dots in band structures are distinguished by red colouring (see Figure 2 e and f), and the top of the valance states in pristine *g*-C_3N_4, and C-dots/*g*-C_3N_4 are shifted to zero. The indirect band gap by HSE06 functional was 3.02 eV, which is comparable to the experiment value.[7] As shown in Figure 2a, the indirect band gap of pristine 2 x2 *g*-C_3N_4 by the PBE functional is 1.89 eV, which is smaller than the experimental value, due to the self-interaction is neglected in the PBE functional. In C-dots/*g*-C_3N_4, the occupied energies levels of C-dots lay within the band gap of *g*-C_3N_4, while the unoccupied C-dots levels lay above the conduction band of *g*-C_3N_4. Distinguished changes are noticed concerning the shapes of valence states and conduction states of *g*-C_3N_4 when it hybridized with C-dots. This phenomenon indicates the strong interactions between C-dots and *g*-C_3N_4, as can be further validated by the interaction energy values. The interaction energy of trigonal C-dot/*g*-C_3N_4 and hexagonal C-dot/*g*-C_3N_4 are 1.58 eV and 1.87 eV, respectively. This clearly indicted the enhanced stability in the hybrid C-dot/*g*-C_3N_4 complex compared to the isolate systems.

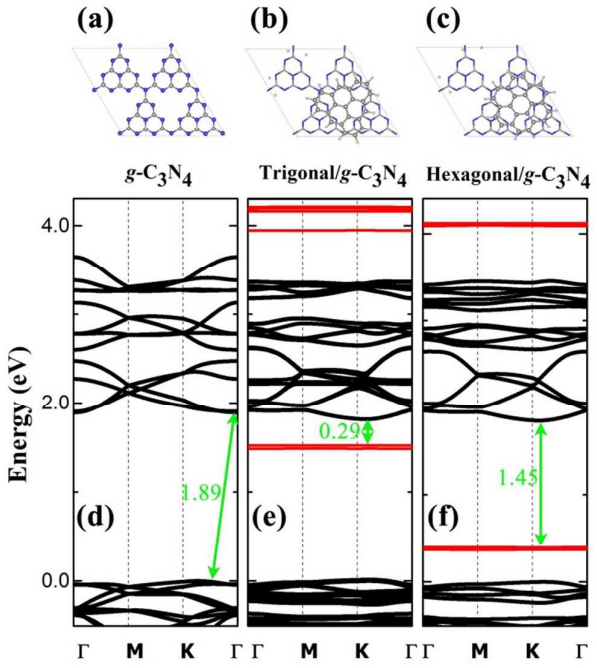

Figure 2 The geometry and band structures of *g*-C_3N_4 and C-dots/*g*-C_3N_4. The energy levels of C-dots are distinguished by red line. In the C-dots/*g*-C_3N_4, the *g*-C_3N_4 is represented by stick model. Atom colour code: carbon (grey), nitrogen (blue), hydrogen (white). To improve legibility, 'C-dot' was omitted from the labels.

The main difference between two C-dot/*g*-C_3N_4 systems is the positions of occupied C-dots energy levels, due to the different magnetic properties of the two group C-dots: trigonal C-dots with a linear scaling net spin, while the hexagonal C-dots with a zero spin[33]. Therefore, the occupied C-dot energy level of trigonal C-dot/*g*-C_3N_4 is close to conduction states of *g*-C_3N_4 with a bandgap of 0.29 eV, while that of hexagonal C-dot/*g*-C_3N_4 is close to valence states of *g*-C_3N_4 with a bandgap of 1.45 eV. The occupied C-dots energy levels coupled with the energy levels of *g*-C_3N_4 lead to a narrower bandgap, so a red shift is expected in optical absorption spectra in the hybrid systems.

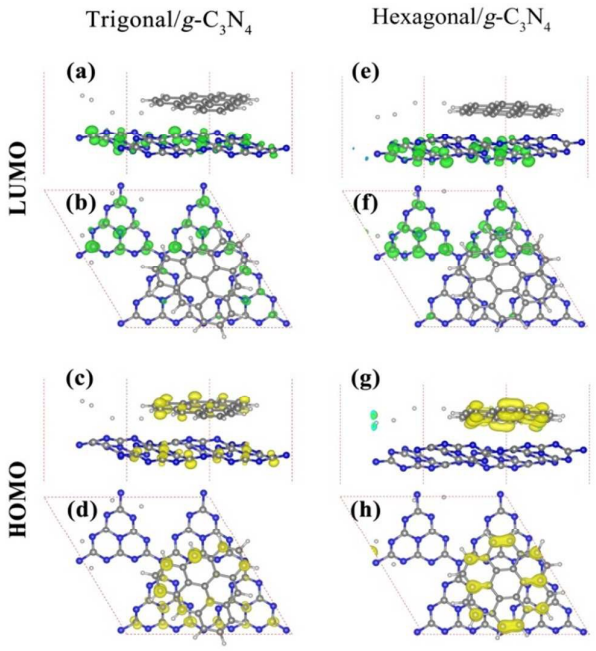

Figure 3 The HOMO and LOMO of C-dots/*g*-C_3N_4 were shown in both side and top views. Atom colour code: carbon (grey), nitrogen (blue), hydrogen (white). To improve legibility, 'C-dot' was omitted from the labels.

The highest occupied molecular orbital (HOMO) and lowest unoccupied molecular orbital (LUMO) of C-dots/*g*-C_3N_4 are plotted in Figure 3. In trigonal C-dot/*g*-C_3N_4, the LUMO is mainly distributed around regions of *g*-C_3N_4 which are not covered by a C-dot. The HOMO is located at interaction area of C-dot and *g*-C_3N_4, which is predominantly distributed on the C-dot and partly on the triangular ring covered by the C-dot, due to the narrow gap of trigonal C-dot/*g*-C_3N_4. In the hexagonal C-dot/*g*-C_3N_4, the LUMO is located on *g*-C_3N_4, while the HOMO is associated with the C-dots. The main difference between trigonal C-dot/g-C3N4 and hexagonal C-dot/g-C3N4 is the charge distribution on HOMO. The HOMO of trigonal C-dot/g-C3N4 is more delocalized due to a net spin in the trigonal C-dots, i.e. the unpaired electrons in trigonal C-dots. However, there is no net spin in hexagonal C-dots and the electrons in hexagonal C-dot/g-C3N4 system are all paired, and its HOMO is more localized. Nevertheless, the HOMO-LUMO in both systems are segregated, which is expected to favour the separation of photogenerated electron and hole pairs spatially.

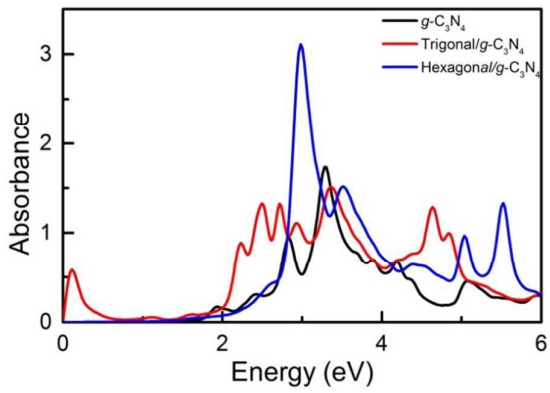

Figure 4 The optical absorption spectra of *g*-C_3N_4 and C-dots/*g*-C_3N_4. The trigonal C-dot and hexagonal C-dot used here is $C_{22}H_{12}$ and $C_{24}H_{12}$, respectively. To improve legibility, 'C-dot' was omitted from the labels.

Calculations of the optical absorption spectra for pristine *g*-C_3N_4 and C-dots/*g*-C_3N_4 are shown in Figure 4. For pristine *g*-C_3N_4, the main light absorption peak located at 3.28 eV and a smaller light absorption peak is located at 2.84 eV. As *g*-C_3N_4 is decorated with trigonal C-dot, there are three new significant absorption peaks which appear, caused by the C-dot at 2.72 eV, 2.49 eV, and 2.23 eV. The absorption peak at 0.12 eV was mainly attributed to the hybridization between C-dots and *g*-C_3N_4. In the hexagonal C-dot/*g*-C_3N_4 system, there is only one dominating absorption peak located at 2.98 eV in the long wavelength range. Therefore, it is highly possible for direct excitation of e^- from HOMO of C-dots to conduction band of *g*-C_3N_4, and then the light absorption is extended into the visible light range in the hybridized C-dots/g-C_3N_4 complex.

The band alignment of isolated C-dots and *g*-C_3N_4 were calculated by the HSE06 method as shown in Figure 5. The CBM potential of isolated *g*-C_3N_4 is -0.88 eV vs NHE, which is more negative than the standard electrode potential H^+/H_2, while the VBM potential is 2.14 eV vs NHE, which is more positive than the standard electrode potentials of both H_2O/O_2 and H_2O_2/O_2. Clearly, the band-edge positions fit the water reduction and oxidation potentials of *g*-C_3N_4. However, the band gap of 3.02 eV is too wide for visible-light absorption. Meanwhile, the HOMOs of C-dots are more negative than the oxidation level of water splitting. Herein, the C-dots cannot

split the water independently. However, the HOMO level of C-dots are in the middle of bandgap of g-C_3N_4, while the C-dot LUMO is above the CBM of g-C_3N_4. This type II band alignment of g-C_3N_4 and C-dots could enhance the visible-light response by hybridizing them together, which is consistent with the results of Figure 2. As the sizes of trigonal and hexagonal C-dots increase, the HOMO moves up while the LUMO moves down in the band alignment, leading to a narrower band gap. In addition, the relative positions of band alignment of g-C_3N_4 and C-dots maintain a type II band alignment. This indicates that a slight enlargement of the C-dots' size could enhance the visible-light response of C-dots/g-C_3N_4.

Combining the band alignment of g-C_3N_4 and C-dots with above analysis, C-dots act as spectral sensitizers in the hybrid C-dots/g-C_3N_4 complex. Additionally, the electrons from the C-dots' HOMO of can be directly photoexcited into the conduction band of the g-C_3N_4 by visible light, which separates the electron and hole into each of the different materials. These remarkable properties are expected to enhance the oxidation/reduction of water into hydrogen.

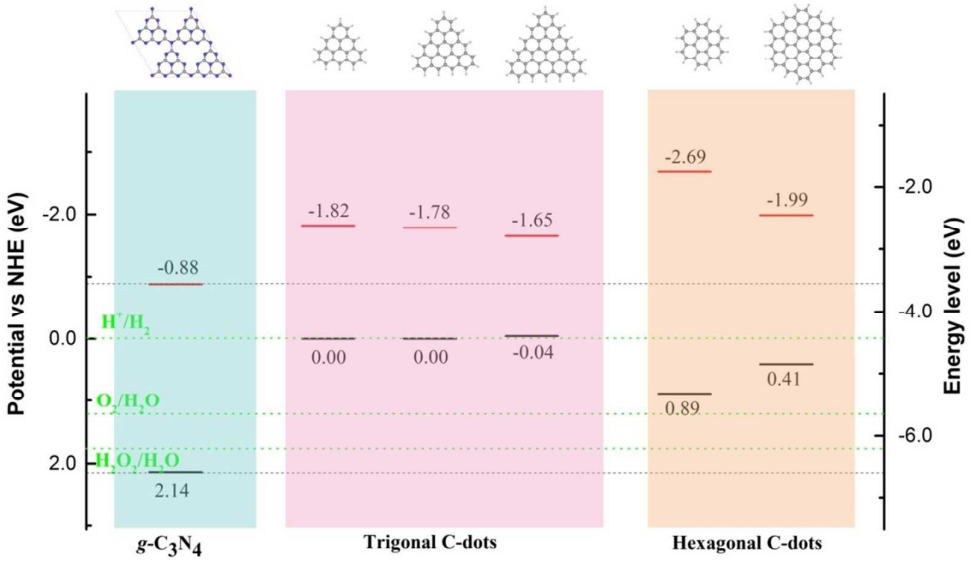

Figure 5 The Calculated VBM (HOMO) and CBM (LUMO) potential versus normal hydrogen electrode of isolated g-C_3N_4 and C-dots by HSE06 method. Atom colour code: carbon (grey), nitrogen (blue), hydrogen (white).

Conclusion

In summary, we have demonstrated that hybridization of g-C_3N_4 with C-dots could form type-II van der Waals heterojunction which enhances the photocatalytic solar water splitting performance of pristine g-C_3N_4. Hybrid C-dots/g-C_3N_4 leads to a narrower bandgap, and a red shift in light absorption spectra. Furthermore, the segregation of the HOMO-LUMO levels favours the separation of photogenerated electron-hole pairs. In addition, the type II band alignment of C-dots and g-C_3N_4 indicates that C-dots might act as spectral sensitizer in the hybrid C-dots/g-C_3N_4 for water splitting.

Acknowledgements

We acknowledge generous grants of high-performance computer time from computing facility at Queensland University of Technology and Australian National Facility. A.D. greatly appreciates the Australian Research Council QEII Fellowship (DP110101239) and financial support of the Australian Research Council under Discovery Project (DP130102420).

Notes and references

1. M. Ni, M. K. H. Leung, D. Y. C. Leung and K. Sumathy, *Renew. Sust. Energ. Rev.*, 2007, **11**, 401-425.
2. A. Fujishima and K. Honda, *Nature*, 1972, **238**, 37-38.
3. A. Kudo and Y. Miseki, *Chem. Soc. Rev.*, 2009, **38**, 253-278.
4. S. Cao and J. Yu, *J. Phys. Chem. Lett.*, 2014, **5**, 2101-2107.
5. S. Yin, J. Han, T. Zhou and R. Xu, *Catal. Sci. Technol.*, 2015, DOI: 10.1039/C5CY00938C.
6. K. Maeda, *J. Photochem. Photobiol. C: Photochem. Rev.*, 2011, **12**, 237-268.
7. X. Wang, K. Maeda, A. Thomas, K. Takanabe, G. Xin, J. M. Carlsson, K. Domen and M. Antonietti, *Nat. mater.*, 2009, **8**, 76-80.
8. Y. Zheng, Y. Jiao, Y. Zhu, L. H. Li, Y. Han, Y. Chen, A. Du, M. Jaroniec and S. Z. Qiao, *Nat. Commun.*, 2014, **5**, 3783.
9. H.-Z. Wu, L.-M. Liu and S.-J. Zhao, *Phys. Chem. Chem. Phys.*, 2014, **16**, 3299-3304.
10. Y. Zhang, T. Mori, L. Niu and J. Ye, *Energy. Environ. Sci.*, 2011, **4**, 4517-4521.
11. X. Ma, Y. Lv, J. Xu, Y. Liu, R. Zhang and Y. Zhu, *J. Phys. Chem. C*, 2012, **116**, 23485-23493.
12. K. Striegler, *Modified Graphitic Carbon Nitrides for Photocatalytic Hydrogen Evolution from Water: Copolymers, Sensitizers and Nanoparticles*, Springer, 2015.
13. G. Liu, P. Niu, C. Sun, S. C. Smith, Z. Chen, G. Q. Lu and H.-M. Cheng, *J. Am. Chem. Soc.*, 2010, **132**, 11642-11648.
14. Y. Zhang, T. Mori, J. Ye and M. Antonietti, *J. Am. Chem. Soc.*, 2010, **132**, 6294-6295.
15. A. Du, S. Sanvito, Z. Li, D. Wang, Y. Jiao, T. Liao, Q. Sun, Y. H. Ng, Z. Zhu and R. Amal, *J. Am. Chem. Soc.*, 2012, **134**, 4393-4397.
16. J. Liu, Y. Liu, N. Liu, Y. Han, X. Zhang, H. Huang, Y. Lifshitz, S.-T. Lee, J. Zhong and Z. Kang, *Science*, 2015, **347**, 970-974.
17. H. Li, L. Zhou, L. Wang, Y. Liu, J. Lei and J. Zhang, *Phys. Chem. Chem. Phys.*, 2015, **17**, 17406-17412.
18. J. Zhang, F. Ren, M. Deng and Y. Wang, *Phys. Chem. Chem. Phys.*, 2015, **17**, 10218-10226.
19. Z. Tachan, I. Hod and A. Zaban, *Adv. Energy Mater.*, 2014, **4**, 1301249.
20. H. Li, Z. Kang, Y. Liu and S.-T. Lee, *J. Mater. Chem.*, 2012, **22**, 24230-24253.
21. H. Li, X. He, Z. Kang, H. Huang, Y. Liu, J. Liu, S. Lian, C. H. A. Tsang, X. Yang and S.-T. Lee, *Angew. Chem. Int. Ed.*, 2010, **49**, 4430-4434.
22. H. Zhang, H. Huang, H. Ming, H. Li, L. Zhang, Y. Liu and Z. Kang, *J. Mater. Chem.*, 2012, **22**, 10501-10506.
23. R. Zhang, S. Qi, J. Jia, B. Torre, H. Zeng, H. Wu and X. Xu, *J. Alloy. Comp.*, 2015, **623**, 186-191.
24. G. Kresse and J. Furthmüller, *Comp. Mater. Sci.*, 1996, **6**, 15-50.
25. G. Kresse and J. Furthmüller, *Phys. Rev. B*, 1996, **54**, 11169.
26. J. P. Perdew, K. Burke and M. Ernzerhof, *Phys. Rev. Lett.*, 1996, **77**, 3865.
27. J. P. Perdew, M. Ernzerhof and K. Burke, *J. Chem. Phys.*, 1996, **105**, 9982-9985.
28. S. Grimme, *J. Comput. Chem.*, 2006, **27**, 1787-1799.
29. H. J. Monkhorst and J. D. Pack, *Phys. Rev. B*, 1976, **13**, 5188.
30. J. Paier, M. Marsman, K. Hummer, G. Kresse, I. C. Gerber and J. G. Ángyán, *J. Chem. Phys.*, 2006, **124**, 154709.
31. C. G. Zoski, *Handbook of electrochemistry*, Elsevier, 2006.
32. S. S. Batsanov, *Inorg. Mater.*, 2001, **37**, 871-885.
33. W. L. Wang, S. Meng and E. Kaxiras, *Nano Lett.*, 2008, **8**, 241-245.